Rendiconti Lincei. Scienze Fisiche e Naturali (2018) 29:209–217
https://doi.org/10.1007/s12210-018-0706-7

THE QUANTUM WORLD OF MOLECULES

Relativistic quantum chemistry involving heavy atoms

Matteo De Santis[1] · **Leonardo Belapassi**[2] · **Francesco Tarantelli**[1] · **Loriano Storchi**[3]

Received: 15 February 2018 / Accepted: 26 April 2018 / Published online: 5 May 2018
© Accademia Nazionale dei Lincei 2018

Abstract
Quantum chemistry is nowadays a term referring to a wide set of theoretical frameworks and models mainly relying on non-relativistic quantum mechanics. While, in most cases, the picture of the molecular structure and of the chemical reality provided by non-relativistic quantum chemistry is appropriate, we live in a universe with a finite speed of light. While neglecting variation of mass and velocity in the interaction of electrons and atomic nuclei is often safe, this is no more the case when heavy atoms are involved. In the present paper, we will briefly review the most rigorous way to include relativity in the modeling of molecular systems, that is to use the full 4-component (4c) formalism derived from the Dirac equation. Specifically, we will review the implementation that has been carried out in an effective 4c code called BERTHA. A recently developed method to gain deep insights into chemical bond is also presented and discussed in the 4c Dirac–Kohn–Sham context, the so-called natural orbitals for chemical valence/charge-displacement analysis.

Keywords Four-component · Relativistic DFT · Chemical bond · Heavy atoms · Relativistic effects

1 Introduction

Since the mid-70s, it was shown that relativistic effects, arising mainly by the fast moving of the core electrons and propagating into the valence region, may become very important for chemical bonding (Pyykkö and Desclaux 1979; Pyykko 1988). It is now universally recognized that relativistic effects play a crucial role in chemistry of heavy elements for their impact on structures, and optical and spectroscopic properties. To mention only a few examples of chemical properties dictated by relativity, we may cite the peculiarities of gold in either homogeneous and heterogeneous catalysis, the liquidity of mercury at room temperature, and lead–acid battery (Pyykkö 2012). Among other effects, spin–orbit coupling plays a crucial role in spectroscopy, affecting both the energetics of the electronic states and the nature of electronic transitions by enabling spin-forbidden excitations. These phenomena are of high relevance in many contexts of modern technology, such as dye-sensitized solar cells, where light absorption may be enhanced using complexes containing heavy elements with strong spin-forbidden transitions (Kinoshita et al. 2012). In addition, in biology, the capability of gold complexes to selectively target protein systems (Casini and Messori 2011) might be ascribed to relativistic effects controlling the metal center reactivity in aqueous media (Theilacker et al. 2015).

The most rigorous way to include relativity in the modeling of molecular systems is surely to use the full 4-component (4c) formalism derived from the Dirac equation (Dirac 1949). This formalism has been developed by Bertha Swirles (1935), who put forward for the first time a multielectron

This contribution is the written, peer-reviewed version of a paper presented at the International Conference "The Quantum World of Molecules: from Orbitals to Spin Networks", held at the Accademia Nazionale dei Lincei in Rome on 27-28 April, 2017.

✉ Leonardo Belapassi
leonardo.belpassi@cnr.it

Francesco Tarantelli
francesco.tarantelli@unipg.it

Loriano Storchi
loriano@storchi.org

[1] Dipartimento di Chimica, Biologia e Biotecnologie, Università degli Studi di Perugia, Via Elce di Sotto 8, 06123 Perugia, Italy

[2] Istituto di Scienze e Tecnologie Molecolari, Consiglio Nazionale delle Ricerche c/o Dipartimento di Chimica, Biologia e Biotecnologie, Università degli Studi di Perugia, Via Elce di Sotto 8, 06123 Perugia, Italy

[3] Istituto di Scienze e Tecnologie Molecolari, Consiglio Nazionale delle Ricerche c/o Dipartimento di Farmacia, Università degli Studi 'G. D'Annunzio', Via dei Vestini 31, 66100 Chieti, Italy

Hamiltonian starting from one particle Dirac equation. A myriad of approximate methods have been derived over the years from the rigorously relativistic 4c equations. Among these, the so-called "2-components" approximation, deriving from the decoupling the "large" and "small" components of the Dirac spinors (Reiher and Wolf 2014), is one of the most used in the calculation of the electronic structure of molecules. Popular 2-component schemes are the Douglas–Kroll–Hess (Reiher and Wolf 2004) and the Zero-Order Regular Approximation hamiltonians (van Lenthe et al. 1996). Both of them have found a wide range of applications with implementations in several modern commercial codes.

The basic motivation for the use of these reduced hamiltonians is mainly of historical origin, with the assumption that full 4c approach is computationally too demanding. We have shown in a series of works that one can greatly reduce the computational burden of a Dirac–Kohn–Sham (DKS) calculation by implementing various parallelization and memory distribution schemes and by introducing new algorithms, such as those based on the "density fitting" method (see Belpassi et al. 2011; Rampino et al. 2014 and references therein). This makes it possible to carry out Density Functional Theory (DFT) calculations at the full relativistic 4c level in an extremely efficient way. New perspectives have, indeed, been opened by the above algorithmic advances, which have represented a leap forward of several order of magnitude in the performance of the full DKS approach. Thus, for instance, we have extended the applicability range of all-electron DKS calculations to large clusters of heavy metals (Rampino et al. 2015). These implementations have been carried out in an effective 4c code: BERTHA. The BERTHA code is basically built around a smart and efficient algorithm for the analytical evaluation of relativistic electronic repulsion integrals, developed by Quiney and Grant in Oxford more than a decade ago (Grant 2007), which represents the relativistic generalization of the well-known McMurchie–Davidson algorithm (Quiney et al. 1997). The basis functions employed are derived from the SGTF (Spherical Gaussian Type Function) basis and are termed G-spinors [see p. 544 of Ref. (Grant 2007)]. G-spinors are designed to have the same transformational properties as central field atomic four-spinors and they are the natural choice when used in combination with a finite-size nuclei model (Ishikawa et al. 1985; Grant and Quiney 1988; Grant 2007). For the sake of completeness, we mention that alternatives to Gaussian-type spinors exist (Grant 2007) (see, for instance, the research activity of Bağcı and Hoggan on the use of S-spinors Bağcı and Hoggan 2016, 2018).

In the present work, we will first briefly recall the general aspects of the DKS 4c approach, as implemented in BERTHA. Then, we will present and discuss some illustrative results related to a recently introduced method to analyze the chemical bond, the so-called NOCV/CD (Natural Orbitals for Chemical Valence/Charge Displacement) analysis that recently has been developed in the specific context of the DKS module of BERTHA (De Santis et al. 2018).

2 The DKS implementation in BERTHA

In the present section, we will briefly cover some of the basic aspects of what can be considered the state of the art for the full 4c DKS formalism (Belpassi et al. 2011).

2.1 The DKS equation and the G-spinor basis functions

In BERTHA, only longitudinal interactions of the DKS equations are considered (Quiney and Belanzoni 2002), and thus, the following simple form is considered:

$$\{c\boldsymbol{\alpha}\cdot\mathbf{p}+\beta c^2+v^{(I)}(\mathbf{r})\}\Psi_i(\mathbf{r})=\varepsilon_i\Psi_i(\mathbf{r}), \tag{1}$$

where, as in the non-relativistic case, the $v^{(I)}(\mathbf{r})$ interaction is divided into three terms: the nuclear potential term, the Coulomb interaction, and an exchange-correlation term:

$$v^{(I)}(\mathbf{r})=v_{ext}(\mathbf{r})+v_H^{(I)}[\rho(\mathbf{r})]+v_{xc}^{(I)}[\rho(\mathbf{r})]. \tag{2}$$

The 4c relativistic DKS code implemented in BERTHA is based on the use of an uncontracted Gaussian basis set expansion. These basis functions, named G-spinors (Grant 2007), is particularly advantageous when is coupled with a finite charge distribution model for the nuclei. They guarantee that the boundary conditions (including at the nuclei position) imposed by the Dirac equation on the ratio of its large- and small-component solutions are satisfied (Grant and Quiney 1988) and do not suffer from the variational problems of kinetic balance (Dyall and Fægri 1990). As finite-nuclei model, we use a spherically symmetric Gaussian charge distribution of the form:

$$\rho_A(r)=Z\left(\frac{\lambda_A}{\pi}\right)^{3/2}\exp\left(-\lambda_A r^2\right), \tag{3}$$

where Z is the nuclear charge and λ_A is a positive constant related to the root-mean-square radius of the nucleus. The latter may be determined by fitting the RMS radius of the Gaussian function to experimental values obtained from electron scattering experiments. In BERTHA, we use the formulas for the nuclear Gaussian exponent, λ_A, suggested by (Visscher and Dyall 1997).

The G-spinors are two-component spin–orbit-coupled objects derived from the Spherical Gaussian Type Function (SGTF) basis (Saunders 1983), and each G-spinor consists of two components, the large (labeled L) and the small (labeled S) one:

$$M_{\mu}^{(L)}(\mathbf{r}) = \frac{f_{\mu}^{(L)}(r)}{r}\chi_{\kappa,m_j}(\theta,\varphi), \tag{4}$$

$$M_{\mu}^{(S)}(\mathbf{r}) = i\frac{f_{\mu}^{(S)}(r)}{r}\chi_{-\kappa,m_j}(\theta,\varphi), \tag{5}$$

where $f_{\mu}^{(T)}(r)$ are radial functions (being T either L or S) and $\chi_{\kappa,m_j}(\theta,\varphi)$ are spin-angular functions (Quiney and Belanzoni 2002) constructed from spherical harmonic functions in a two-component space of spin eigenfunctions. Each $M_{\mu}^{(T)}(\mathbf{r})$ is a Gaussian-based two-component object labeled by a μ index mapping univocally onto the set of parameters (Gaussian center and exponent, fine-structure quantum number, and magnetic quantum number) necessary to completely characterize the function.

Once the G-spinors basis functions have been introduced, the eigenvalue equation which we need to solve at each self-consistent-field (SCF) iteration is as follows:

$$\boldsymbol{H}_{\mathrm{DKS}}\begin{bmatrix}\boldsymbol{c}^{(\mathrm{L})}\\ \boldsymbol{c}^{(\mathrm{S})}\end{bmatrix} = E\begin{bmatrix}\boldsymbol{S}^{(\mathrm{LL})} & 0\\ 0 & \boldsymbol{S}^{(\mathrm{SS})}\end{bmatrix}\begin{bmatrix}\boldsymbol{c}^{(\mathrm{L})}\\ \boldsymbol{c}^{(\mathrm{S})}\end{bmatrix} \tag{6}$$

being $\boldsymbol{c}^{(\mathrm{T})}$ the spinor expansion vectors and $\boldsymbol{H}_{\mathrm{DKS}}$ the DKS matrix, that is the matrix representation of the DKS operator in the G-spinor basis:

$$\begin{bmatrix}\boldsymbol{v}^{(\mathrm{LL})}+\boldsymbol{J}^{(\mathrm{LL})}+\boldsymbol{K}^{(\mathrm{LL})}+mc^2\boldsymbol{S}^{(\mathrm{LL})} & c\boldsymbol{\Pi}^{(\mathrm{LS})}\\ c\boldsymbol{\Pi}^{(\mathrm{SL})} & \boldsymbol{v}^{(\mathrm{SS})}+\boldsymbol{J}^{(\mathrm{SS})}+\boldsymbol{K}^{(\mathrm{SS})}-mc^2\boldsymbol{S}^{(\mathrm{SS})}\end{bmatrix}. \tag{7}$$

In Eq. 7, one recognizes the basis representations of the nuclear ($\boldsymbol{v}$), Coulomb ($\boldsymbol{J}$), and exchange-correlation potentials ($\boldsymbol{K}$), being $\boldsymbol{S}$ and $\boldsymbol{\Pi}$ the overlap and kinetic energy operator matrix, respectively. For a more detailed description of the formalism, the reader may refer to Belpassi et al. (2011) and references therein.

2.2 The SCF procedure

The key points of a typical DKS single-point calculation, as in any SCF iterative procedure, is the DKS matrix construction, reported in Eq. 7, and the subsequent diagonalization, see Eq. 6. Starting from an initial tentative density guess, which is usually the superposition of the atomic densities, the SCF iterations begin. Each iteration can be subdivided into three main steps: (1) density fitting, (2) DKS matrix construction, and (3) linear algebra step, where the DKS matrix is diagonalized; and the new density is determined. As pointed out above, the two most demanding steps are the DKS matrix construction and the subsequent diagonalization. In regard to the former, the adoption of a density fitting approach has represented an indisputable leap forward in lowering the computational cost of the entire procedure. As has been already mentioned, in BERTHA, the spinor solutions of the DKS equation are expanded as a linear combination of Gaussian G-spinor basis functions. This allows an exact evaluation of the density elements as a finite linear combination of standard Hermite Gaussian-type functions (HGTF). This formulation enables a highly efficient analytic evaluation of all the required multi-center G-spinor interaction integrals. The overall efficiency of the procedure has been further enhanced by the choice of the fitting basis set as primitive HGTFs of common exponents and spanning all angular momenta. This approach was found to be particularly effective when high angular momenta are necessary, which is, indeed, the case for molecular systems containing heavy elements. The density fitting scheme has been shown to reduce the scaling power for the construction of the DKS matrix from $O(N^4)$ to $O(N^3)$ reducing enormously also the prefactor without appreciable effects on the accuracy (Belpassi et al. 2008b).

The current version of the BERTHA software has been fully parallelized in all its component computational steps. This is important, because, as it is well known, Amdahl's law (Amdahl 1967) poses an upper limit to the reachable speed-up of a code which is determined by its serial portion. Having fully parallelized BERTHA has removed such upper limit, with very satisfactory results (Rampino et al. 2014). Indeed, not only molecular system such as the Au_{32}, with more than 25,000 basis functions, are now workable, but given an adequate number of computational nodes/CPUs almost any molecular system is affordable in terms of computing time requirements. We were also able to remove the further limiting factor represented by fast memory requirements, which is also a key aspect for the feasibility of accurate all-electron treatment of multi-heavy-atom systems. For example, in the cited Au_{32} gold cluster, using a relatively small G-spinor basis set derived by decontracting the double-ζ quality basis set of Dyall (2004) and Dyall and Gomes (2010), the memory usage is higher than 23 GiB. To tackle this, the current version of BERTHA is using a fully distributed memory implementation where the SCF procedure is replicated on all the parallel processes, and each process is working on subsets of the global matrices (Rampino et al. 2014). In conclusion, our approach, being both CPU time and memory scalable with the number of processors used, virtually overcomes at once both time and memory barriers associated with 4c DKS calculations.

3 The NOCV/CD analysis in the DKS 4c context

A true understanding of chemical bonds is often difficult to attain, and this is all the more so far many-electron complex systems containing heavy metals. To tackle this

problem, with particular reference to the relativistic 4c framework, we have recently developed the NOCV/CD method of analysis, which aims to give a concise and insightful picture of the electronic molecular structures obtained within the DKS theory (De Santis et al. 2018). In the following, we shall illustrate how the implementation of this tool in this specific context is of great help to easily visualize and understand relativistic effects in the chemical bond.

We begin by recalling the Charge-Displacement (CD) analysis, that has already been employed in different scenarios (Belpassi et al. 2008a). The CD function is defined as a partial integration along a suitable z axis of the difference $\Delta\rho(x, y, z')$ between the electron density of a molecular system and that of its non-interacting fragments, imagined to lie in the same spatial position which they occupy in the adduct:

$$\Delta q(z) = \int_{-\infty}^{z} \mathrm{d}z' \int_{-\infty}^{\infty}\int_{-\infty}^{\infty} \Delta\rho(x, y, z')\mathrm{d}x\mathrm{d}y. \tag{8}$$

In the previous equation, the integration axis z is obviously chosen according to some physical criteria: for instance, the bond axis between two fragments. The CD function so defined represents, at each point z the charge transferred, upon formation of the molecule, across a perpendicular plane through z. It has positive value if the charge flows from right to left (towards decreasing z), and negative for the opposite direction.

The electron density difference can be very easily partitioned in additive symmetry components when both the adduct and its constituting fragments belong to the same symmetry group. This induces a similar useful decomposition of the CD function which can be used to obtain, for example, a precise picture of donation and back-donation charges (Zuccaccia et al. 2013). However, it is clear that such symmetry decomposition cannot be applied in the majority of cases, especially for the large systems typically governed by relativistic effects. The NOCV/CD approach overcomes this limitation by providing a decomposition of $\Delta\rho$ in terms of contributions arising from the molecular spinors most involved in the bonding. Natural Orbitals for Chemical Valence (NOCV) were introduced by Mitoraj and Michalak (2007) as descriptors of chemical bond. The formalism allows a very compact description of the bonding phenomenon, because the electron density difference $\Delta\rho$ can be brought into diagonal contributions in terms of NOCVs. This only requires at the outset a slightly different definition of the reference density ρ^0, which is no longer the simple sum of the densities of the non-interacting fragments, but is instead, following the theory of Nalewajski et al. (1993, 1997) and Nalewajski and Mrozek (1994), obtained from the occupied spinors of non-interacting fragments properly orthogonalized to each other and renormalized. We shall refer to this new set of spin-orbitals as $\mathbf{\Psi}_i^0$. In this scheme, the fictitious wavefunction associated with ρ^0 is the so-called promolecule, because rather than two separate wavefunctions, their antisymmetrized product is taken as reference.

The NOCV are defined as eigenfunctions of the following valence operator:

$$\hat{V} = \sum_{i=1}^{N} (|\mathbf{\Psi}_i^{(AB)}\rangle\langle\mathbf{\Psi}^{(AB)}| - |\mathbf{\Psi}_i^0\rangle\langle\mathbf{\Psi}_i^0|), \tag{9}$$

that is, the difference between the adduct and the newly defined reference density operators. The resulting density rearrangement called $\Delta\rho'$ now reads:

$$\Delta\rho' = \sum_{i}^{N} |\mathbf{\Psi}_i^{(AB)}|^2 - \sum_{i}^{N} |\mathbf{\Psi}_i^0|^2. \tag{10}$$

Now, we exploit the pairing property of the NOCVs, consisting in the fact that all non-zero eigenvalues of $\hat{V}$ appear in pairs of opposite numbers:

$$\hat{V}|\varphi_{\pm k}\rangle = \pm v_k|\varphi_{\pm k}\rangle \quad (v_k > 0), \tag{11}$$

so that the density rearrangement is brought into diagonal contributions in terms of the NOCV:

$$\Delta\rho' = \sum_{k} v_k(|\varphi_k|^2 - |\varphi_{-k}|^2) = \sum_{k} \Delta\rho'_k. \tag{12}$$

This relation guides us in the interpretation of the NOCVs and their associated eigenvalues: upon formation of the adduct from the promolecule, a fraction v_k of electrons is transferred from φ_{-k} to the orbital φ_k. It can be shown from the definition of the operator $\hat{V}$ that k ranges from 1 to the number of occupied spinors. Moreover, it is important to notice that only a small subset of these NOCV pairs actually contributes to the overall rearrangement $\Delta\rho'$, because a large part of them presents values of v_k close to zero. $\Delta\rho$ and $\Delta\rho'$ are slightly different quantities; nevertheless, it has been proved that the analysis based on $\Delta\rho$ and that based on $\Delta\rho'$ lead to the same results (Bistoni et al. 2015).

3.1 A test case: the ClAu–CO bond

Carbon monoxide plays a crucial role as ligand in all of coordination chemistry (Huheey et al. 1993), its importance being exemplified by the sole consideration of its poisonous effect in mammals resulting from Fe–CO complex formation. We shall focus here our attention on the ClAu–CO bond (Evans et al. 2001; Fortunelli and Germano 2000; Belli Dell'Amico et al. 1987), as an example

of the treatment of electron correlation and relativistic effects necessary for the correct quantum chemistry description of heavy-metal chemistry.

The coordination bond of carbon monoxide with metals is generally described in terms of the Dewar–Chatt–Duncanson (DCD) model (Dewar 1951; Chatt and Duncanson 1953; Frenking 2001; Bistoni et al. 2016), whereby the interaction results from donation of electron charge from carbon's lone pair to the empty metal (M) σ orbitals and back-donation from M to the empty CO orbitals of π symmetry (see Bistoni et al. 2016 and references therein for an extensive illustration). In the present section, we shall discuss this by applying the NOCV/CD analysis to the Au–CO bond, a case where relativistic effects are known to play a fundamental role. The calculations were carried out with the full-parallel version of BERTHA. As already mentioned, a finite charge distribution model is employed for the nuclei (Quiney and Belanzoni 2002). The large component of the G-spinor basis set for Au was generated by uncontracting the triple-ζ quality Dyall's basis sets (Dyall 2004; Dyall and Gomes 2010; Dyall 2012, 2007) augmented with the related polarization and correlating functions. The final basis set for Au is thus (30*s*24*p*15*d*11*f*5*g*1*h*). The large component basis functions for C, O, and Cl were instead derived by decontracting the related aug-cc-pVTZ-DK (Dunning 1989; Kendall et al. 1992; Balabanov and Peterson 2005) basis sets available at the "Basis Set Exchange" site (Schuchardt et al. 2007). The corresponding small-component basis was generated using the restricted kinetic balance relation (Grant and Quiney 2000). For the gold atom, a previously optimized auxiliary basis set for the density fitting denoted as B20 (Belpassi et al. 2006) was used. For all other elements, namely, C, O, and Cl, accurate auxiliary basis set was generated using a simple procedure starting from available DeMon Coulomb fitting basis set. It is worth recalling that the HGTFs used as fitting functions are grouped together in sets sharing the same exponents [an analogous scheme is adopted in the non-relativistic DFT code DeMon (Köster and Salahub 2016)]. The sets are formed, so that to an auxiliary function of a given angular momentum all the functions of smaller angular momentum are associated. Consequently, due to the variational nature of the density fitting procedure implemented, a fitting basis set of increased accuracy can be generated by simply up-shifting the angular momentum in the basis set definition. For all lighter atoms, we obtained a fitting basis set of higher accuracy (referred to as A2) simply by up-shifting of two units the angular momentum of all the DeMon Coulomb Fitting definitions. In a previous study, we have showed that the basis set employed here are close to the basis set limit and the NOCVs eigenvalues (and the related CD curves) are in quantitative agreement with those obtained using Slater-type basis with the ADF code (De Santis et al. 2018). Finally, the BLYP functional made of the Becke 1988 (B88) exchange (Becke 1988) plus the Lee–Yang–Parr (LYP) correlation (Lee et al. 1988) was used. An energy convergence criterion of 10^{-7} Hartree on the total energy was adopted. All data were obtained starting from a single-point calculation at the gas-phase experimental equilibrium geometry from Evans et al. (2001) (designated as $r_m^{(2)}$ in Table 4 of the cited reference).

3.1.1 NOCV/CD analysis results and discussion

In the following, we will discuss the theoretical aspects of the ClAu–CO bond in the AuCl(CO) molecule using the previously introduced NOCV/CD analysis. The two non-interacting fragments which one needs to consider are, in this case, CO and AuCl, and the bond axis is used as integration axis for the CD analysis.

We first report, in Table 1, the NOCV charge-transfer (CT) values CT_k, together with their corresponding v_k (see Eq. 11). It should be recalled that, to define CT values in the context of CD analysis, we need to take the CD value at some specific point z between the fragments, i.e., define a plane separating them. The usual choice is the z point where equal-valued isodensity surfaces of the isolated fragments become tangent.

In Fig. 1, we displayed the isodensity surfaces of $\Delta\rho$, $\Delta\rho'$, as explained in Sect. 3, and $\Delta\rho^{\text{anti}}$, the latter defined as the difference between the former two: $\Delta\rho^{\text{anti}} = \Delta\rho - \Delta\rho'$. Thus, $\Delta\rho^{\text{anti}}$ is the density rearrangement occurring upon going from the separate A and B fragments to the promolecule. As has been discussed by Mitoraj et al. (2009), this contribution removes the orbital overlap between the two fragments, shifting charge density from the inter-fragment region towards the fragments. In the figure, blue surfaces represent charge density accumulation, while red ones represent charge depletion. Also displayed in Fig. 1 are the four most significant component NOCV pairs ($\Delta\rho'_1$, $\Delta\rho'_2$, $\Delta\rho'_3$, and $\Delta\rho'_4$). They represent the main contribution to the total

Table 1 Values of v_k and CT_k corresponding to $\Delta\rho_k$ for AuCl(CO)

	v_k	CT_k/e	v_k [a]	CT_k/e [a]
$\Delta\rho$	–	− 0.106	–	− 0.134
$\Delta\rho'$	–	− 0.095	–	− 0.123
$\Delta\rho'_1$	0.507	0.247	0.364	0.184
$\Delta\rho'_2$	0.478	− 0.190	0.398	− 0.137
$\Delta\rho'_3$	0.431	− 0.121	0.397	− 0.137
$\Delta\rho'_4$	0.183	− 0.035	0.211	− 0.037
$\Delta\rho'_5$	0.052	0.001	0.036	0.002
$\Delta\rho'_6$	0.046	0.001	0.036	0.002

The total charge transfers (CT) for $\Delta\rho$ and $\Delta\rho'$ are also reported. On the right panel (i.e., [a] data), we are reporting values obtained with DKS calculation increasing the speed of light by one order of magnitude ($\tilde{c} = 10{\cdot}c$) to approximate the non-relativistic hamiltonian

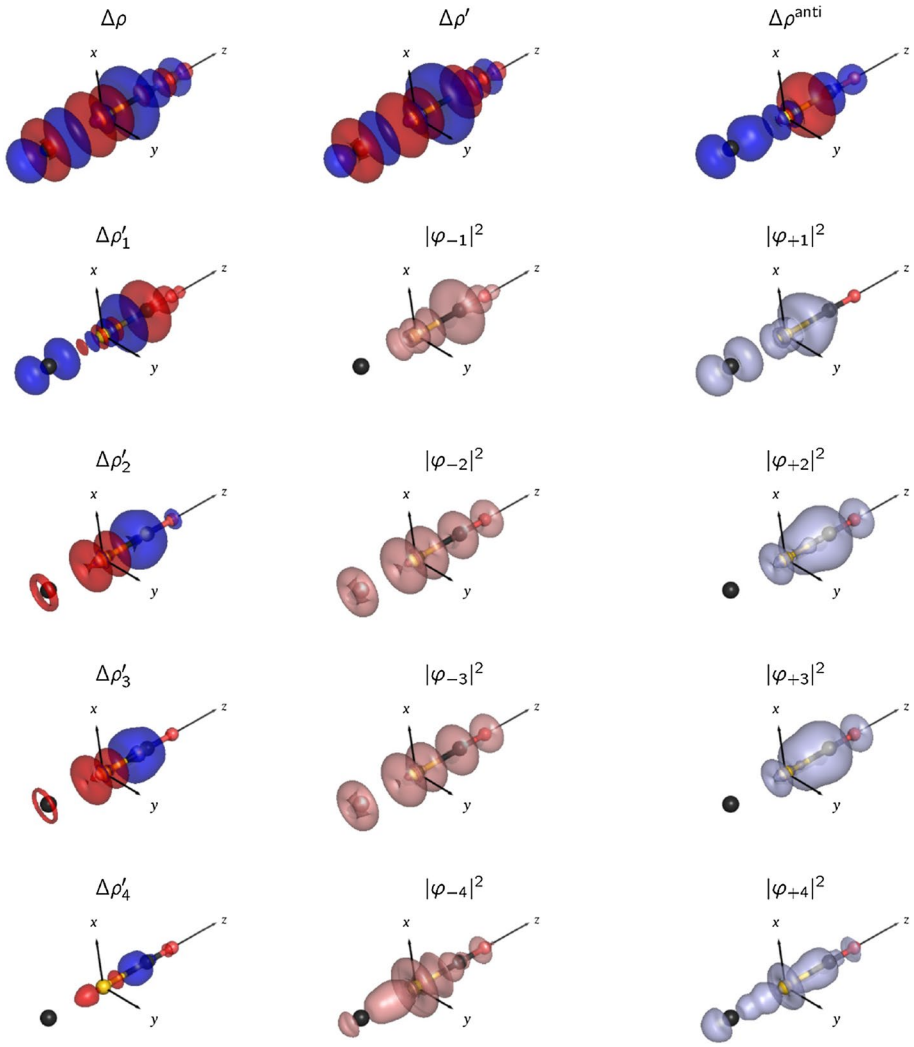

Fig. 1 Isodensity surfaces for $\Delta\rho$, $\Delta\rho'$, and $\Delta\rho_{anti}$ and the contribution to deformation density, $\Delta\rho'$, of the four most significant NOCV pairs ($\Delta\rho'_1$, $\Delta\rho'_2$, $\Delta\rho'_3$, and $\Delta\rho'_4$,) are depicted as isodensity surfaces (±0.0014 a.u). Red surfaces identify charge depletion areas; blue surfaces identify charge accumulation areas. Distinct NOCV pairs components $\{|\varphi_{-k}|^2, |\varphi_k|^2\}$, with $k = 1, 2, 3, 4$, are also shown by means of isodensity surfaces (± 0.005 a.u)

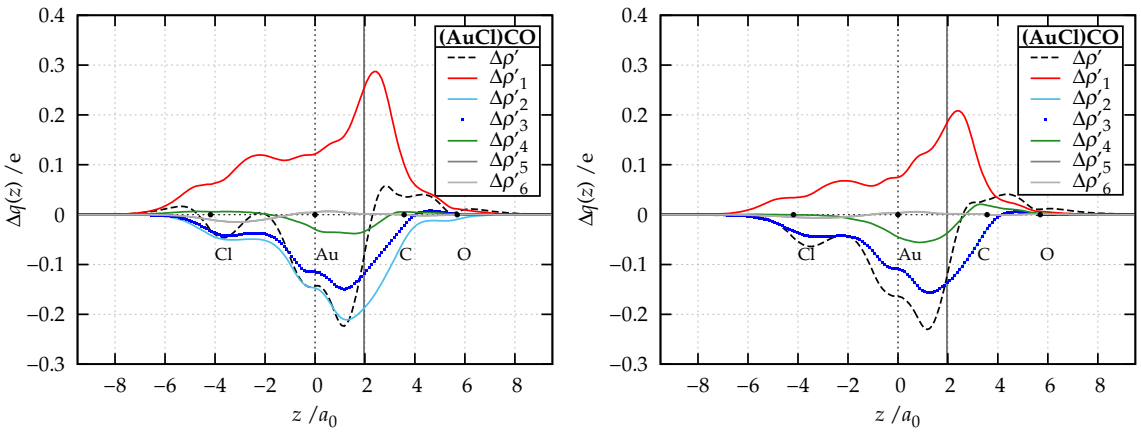

Fig. 2 CD functions associated with the six $\Delta\rho'_k$ components for AuCl(CO) evaluated using the NOCV implementation in BERTHA (left). On the right, the CD functions for AuCl(CO) obtained with DKS calculation increasing the speed of light of one order of magnitude ($\tilde{c} = 10 \cdot c$) to approximate the non-relativistic hamiltonian

$\Delta\rho'$ and the corresponding isodensity surfaces are denoted as $\Delta\rho'_k$.

Finally, in Fig. 2, all the CD functions associated with the first six $\Delta\rho'_k$ components are reported, together with the total $\Delta\rho'$ CD curve.

The CD function clearly shows a substantial ligand-to-metal donation component (labeled as $\Delta\rho'_1$, red curve in the plots) which is positive in the M-carbon region and two components (labeled as $\Delta\rho'_2$ and $\Delta\rho'_3$, the light blue continuous line and the blue dotted line, respectively) which are negative and identify the AuCl moiety-to-ligand back-donation. Remarkably, both donation and back-donation components exhibit absolute maximum and minimum, respectively, near the isodensity boundary. Thanks to the visual inspection of the isodensity-surface plots of $\Delta\rho'_k$ on the left column in Fig. 1, we can assess more precisely many subtle features of these components. For instance, the NOCV-pair density $\Delta\rho'_1$ represents the donation from HOMO of CO fragment to the AuCl moiety. Charge accumulation occurs especially on the site of chlorine and in the inter-fragment region near the gold site, where a blue lobe faces towards the red lobe of CO fragment. Thus, in the corresponding CD curve, a net maximum appears in the same neighborhood of the inter-fragment region. As already stated, the CD curves corresponding to $\Delta\rho'_2$ and $\Delta\rho'_3$ both account for back-donation from AuCl to CO moiety. These curves turn out to be well resolved, especially in the inter-fragment region, displaying different value of their respective charge transfer (see Table 1). The absolute minimum for each curve occurs in the neighborhood, where blue and red lobes oppose each other in the respective $\Delta\rho'_k$. Remarkably, their behavior is qualitatively different in the CO fragment. The former has tiny positive slope at the O atom, so that a small blue lobe appears in the corresponding isodensity-surface plot. Conversely, the latter has positive and close to zero values and displays a tiny local maximum in the CO bonding region. This small effect is due to the polarization of the CO fragment, which "feels" a partial positive charge from AuCl.

As already discussed in the previous work (De Santis et al. 2018), the splitting of the back-donation curves is due to the relativistic spin–orbit coupling, which propagates to the bonding region. The right panel of Fig. 2 confirms this picture. Here, we show the CD curves obtained by increasing the speed of light by an order of magnitude. It can be readily seen that the back-donation curves become nearly overlapping. This is quantitatively shown also by the almost degenerate values of both CT and NOCV eigenvalues reported in the right panel of Table 1. Moreover, on the CO moiety, they only account for the tiny polarization effect. It is quite interesting to note that, in such non-relativistic limit, the general trend of the curves, particularly for the donation component, is retained, even though the absolute values are affected.

4 Conclusions

In the present work, we briefly reviewed the fundamental steps undertaken to overcome time and the memory bottlenecks that in the past have restricted the applicability of all-electron 4c relativistic DFT approaches. This has enabled our program BERTHA to provide the accurate all-electron treatment of chemical systems containing many heavy atoms, making it the ideal starting point for further development of 4c DKS methods. A very useful development in this context is the so-called NOCV/CD analysis discussed here, which can be used to provide insights into the nature of the chemical bonds, in high spin–orbit coupling regime, particularly when heavy atoms are involved. We showed, in particular, that the NOCV/CD approach, used in the framework of relativistic four-component calculations, is suitable to single out the donation and back-donation charge fluxes of the Dewar–Chatt–Duncanson bonding model, which is ubiquitous in the coordination chemistry. We have shown the ability of the NOCV/CD analysis to describe and explain the ClAu–CO bond in the AuCl(CO) molecule. Relativistic effects have a key impact on the bond components and our method highlighted a splitting of the metal to ligand back-donation component induced by the spin–orbit coupling that, starting from the metal, extends to the CO bond. This analysis is particularly valuable to rationalize relativistic effects, including the spin–orbit coupling, on the bonding and permits an easy identification of the main relativistic effects on the coordination bond, by simply "switching off" relativity through the fictitious increase of the speed of light.

Acknowledgements We thank MIUR and the University of Perugia for the financial support of the AMIS project through the program "Dipartimenti di Eccellenza". LS thanks University of Chieti-Pescara for the financial support.

References

Amdahl GM (1967) Validity of the single processor approach to achieving large scale computing capabilities. In: Proceedings of the April 18–20, 1967, spring joint computer conference, ACM, pp 483–485

Bağcı A, Hoggan PE (2016) Solution of the dirac equation using the rayleigh-ritz method: flexible basis coupling large and small components. Results for one-electron systems. Phys Rev E 94:013302. https://doi.org/10.1103/PhysRevE.94.013302

Bağcı A, Hoggan PE (2018) Analytical evaluation of relativistic molecular integrals i Auxiliary functions. Rend Fis Acc Lincei 29(1):191–197. https://doi.org/10.1007/s12210-018-0669-8

Balabanov NB, Peterson KA (2005) Systematically convergent basis sets for transition metals. I. All-electron correlation consistent basis sets for the 3d elements Sc–Zn. J Chem Phys 123(6):064107

Becke AD (1988) Density-functional exchange-energy approximation with correct asymptotic behavior. Phys Rev A 38:3098–3100. https://doi.org/10.1103/PhysRevA.38.3098

Belli Dell'Amico D, Calderazzo F, Dantona R, Straehle J, Weiss H (1987) Olefin complexes of gold (i) by carbonyl displacement from carbonylgold (i) chloride. Organometallics 6(6):1207–1210

Belpassi L, Tarantelli F, Sgamellotti A, Quiney HM (2006) Electron density fitting for the Coulomb problem in relativistic density-functional theory. J Chem Phys 124(12):124104. https://doi.org/10.1063/1.2179420

Belpassi L, Infante I, Tarantelli F, Visscher L (2008a) The chemical bond between Au(I) and the noble gases. comparative study of NgAuF and NgAu^+ (Ng = Ar, Kr, Xe) by density functional and coupled cluster methods. J Am Chem Soc 130(3):1048–1060. https://doi.org/10.1021/ja0772647

Belpassi L, Tarantelli F, Sgamellotti A, Quiney HM (2008b) Poisson-transformed density fitting in relativistic four-component Dirac–Kohn–Sham theory. J Chem Phys 128(12):124108. https://doi.org/10.1063/1.2868770

Belpassi L, Storchi L, Quiney HM, Tarantelli F (2011) Recent advances and perspectives in four-component Dirac–Kohn–Sham calculations. Phys Chem Chem Phys 13:12368–12394. https://doi.org/10.1039/C1CP20569B

Bistoni G, Rampino S, Tarantelli F, Belpassi L (2015) Charge-displacement analysis via natural orbitals for chemical valence: charge transfer effects in coordination chemistry. J Chem Phys 142(8):084112. https://doi.org/10.1063/1.4908537

Bistoni G, Rampino S, Scafuri N, Ciancaleoni G, Zuccaccia D, Belpassi L, Tarantelli F (2016) How π back-donation quantitatively controls the co stretching response in classical and non-classical metal carbonyl complexes. Chem Sci 7:1174–1184. https://doi.org/10.1039/C5SC02971F

Casini A, Messori L (2011) Molecular mechanisms and proposed targets for selected anticancer gold compounds. Curr Top Med Chem 11(21):2647–2660

Chatt J, Duncanson LA (1953) Olefin co-ordination compounds. Part III. Infra-red spectra and structure: attempted preparation of acetylene complexes. J Chem Soc 28:2939–2942

De Santis M, Rampino S, Quiney HM, Belpassi L, Storchi L (2018) Charge-displacement analysis via natural orbitals for chemical valence in the four-component relativistic framework. J Chem Theory Comput. https://doi.org/10.1021/acs.jctc.7b01077

Dewar MJS (1951) A review of π complex theory. Bull Soc Chim Fr 18:C71–79

Dirac PA (1949) Forms of relativistic dynamics. Rev Mod Phys 21(3):392

Dunning TH (1989) Gaussian basis sets for use in correlated molecular calculations. I. The atoms boron through neon and hydrogen. J Chem Phys 90(2):1007–1023. https://doi.org/10.1063/1.456153

Dyall K (2012) Core correlating basis functions for elements 31–118. Theor Chem Acc 131(5):1–11. https://doi.org/10.1007/s00214-012-1217-8. http://dirac.chem.sdu.dk **(basis sets are available from the Dirac web site)**

Dyall KG (2004) Relativistic double-zeta, triple-zeta, and quadruple-zeta basis sets for the 5*d* elements Hf–Hg. Theor Chem Acc 112(5-6):403–409. https://doi.org/10.1007/s00214-004-0607-y. http://dirac.chem.sdu.dk/basisarchives/dyall/ **(basis sets are available from the Dirac web site)**

Dyall KG (2007) Relativistic double-zeta, triple-zeta, and quadruple-zeta basis sets for the 4d elements Y–Cd. Theor Chem Acc 117(4):483–489

Dyall KG, Fægri K (1990) Kinetic balance and variational bounds failure in the solution of the dirac equation in a finite gaussian basis set. Chem Phys Lett 174(1):25–32

Dyall KG, Gomes AS (2010) Revised relativistic basis sets for the 5*d* elements Hf–Hg. Theor Chem Acc 125(1-2):97–100. https://doi.org/10.1007/s00214-009-0717-7. http://dirac.chem.sdu.dk/basisarchives/dyall/ **(basis sets are available from the Dirac web site)**

Evans CJ, Reynard LM, Gerry MC (2001) Pure rotational spectra, structures, and hyperfine constants of OC-AuX (X = F, Cl, Br). Inorg Chem 40(24):6123–6131

Fortunelli A, Germano G (2000) Ab initio study of the intra- and intermolecular bonding in AuCl(CO). J Phys Chem A 104(46):10834–10841

Frenking G (2001) Understanding the nature of the bonding in transition metal complexes: from dewar's molecular orbital model to an energy partitioning analysis of the metal-ligand bond. J Organomet Chem 635(1):9–23

Grant IP (2007) Relativistic quantum theory of atoms and molecules: theory and computation. Springer, Berlin (Springer series on atomic, optical, and plasma physics)

Grant IP, Quiney HM (1988) Foundations of the relativistic theory of atomic and molecular structure. Advances in atomic and molecular physics, vol 23. Academic Press, Cambridge, pp 37 – 86. https://doi.org/10.1016/S0065-2199(08)60105-0

Grant IP, Quiney HM (2000) Rayleigh-Ritz approximation of the Dirac operator in atomic and molecular physics. Phys Rev A 62:022508. https://doi.org/10.1103/PhysRevA.62.022508

Huheey J, Keiter E, Keiter R (1993) Inorganic chemistry, 4th edn. Harper Collins, New York, NY

Ishikawa Y, Baretty R, Binning R (1985) Relativistic Gaussian basis set calculations on one-electron ions with a nucleus of finite extent. Chem Phys Lett 121(1):130–133. https://doi.org/10.1016/0009-2614(85)87169-4

Kendall RA, Dunning TH Jr, Harrison RJ (1992) Electron affinities of the first-row atoms revisited. Systematic basis sets and wave functions. J Chem Phys 96(9):6796–6806

Kinoshita T, Ji Fujisawa, Nakazaki J, Uchida S, Kubo T, Segawa H (2012) Enhancement of near-ir photoelectric conversion in dye-sensitized solar cells using an osmium sensitizer with strong spin-forbidden transition. J Phys Chem Lett 3(3):394–398

Köster AM, Salahub DR et al (2016) demon2k, version 4, the demon developers. http://www.demon-software.com/public_html/program.html. Accessed 14 Feb 2018

Lee C, Yang W, Parr RG (1988) Development of the Colle-Salvetti correlation-energy formula into a functional of the electron density. Phys Rev B 37:785–789. https://doi.org/10.1103/PhysRevB.37.785

van Lenthe EV, Snijders J, Baerends E (1996) The zero-order regular approximation for relativistic effects: the effect of spin-orbit coupling in closed shell molecules. J Chem Phys 105(15):6505–6516

Mitoraj MP, Michalak A, Ziegler T (2009) A combined charge and energy decomposition scheme for bond analysis. J Chem Theory Comput 5(4):962–975. https://doi.org/10.1021/ct800503d

Mitoraj MMA (2007) Natural orbitals for chemical valence as descriptors of chemical bonding in transition metal complexes. J Mol Model 13:347–355

Nalewajski RF, Mrozek J (1994) Modified valence indices from the two-particle density matrix. Int J Quantum Chem 51(4):187–200. https://doi.org/10.1002/qua.560510403

Nalewajski RF, Köster AM, Jug K (1993) Chemical valence from the two-particle density matrix. Theor Chem Acc 85(6):463–484. https://doi.org/10.1007/BF01112985

Nalewajski RF, Mrozek J, Michalak A (1997) Two-electron valence indices from the Kohn–Sham orbitals. Int J Quantum Chem 61(3):589–601

Pyykko P (1988) Relativistic effects in structural chemistry. Chem Rev 88(3):563–594

Pyykkö P (2012) Relativistic effects in chemistry: more common than you thought. Annu Rev Phys Chem 63:45–64

Pyykkö P, Desclaux JP (1979) Relativity and the periodic system of elements. Acc Chem Res 12(8):276–281. https://doi.org/10.1021/ar50140a002

Quiney H, Skaane H, Grant I (1997) Relativistic calculation of electromagnetic interactions in molecules. J Phys B At Mol Opt 30(23):L829

Quiney HM, Belanzoni P (2002) Relativistic density functional theory using Gaussian basis sets. J Chem Phys 117(12):5550–5563. https://doi.org/10.1063/1.1502245

Rampino S, Belpassi L, Tarantelli F, Storchi L (2014) Full Parallel Implementation of an all-electron four-component Dirac–Kohn–Sham program. J Chem Theory Comput 10(9):3766–3776. https://doi.org/10.1021/ct500498m

Rampino S, Storchi L, Belpassi L (2015) Gold-superheavy-element interaction in diatomics and cluster adducts: a combined four-component Dirac–Kohn–Sham/charge-displacement study. J Chem Phys 143(2):024307

Reiher M, Wolf A (2004) Exact decoupling of the Dirac Hamiltonian. II. The generalized Douglas-Kroll-Hess transformation up to arbitrary order. J Chem Phys 121(22):10945–10956

Reiher M, Wolf A (2014) Relativistic quantum chemistry: the fundamental theory of molecular science. Wiley, Hoboken

Saunders V (1983) Molecular integrals for Gaussian type functions. In: Methods in computational molecular physics, Springer, New York, pp 1–36

Schuchardt KL, Didier BT, Elsethagen T, Sun L, Gurumoorthi V, Chase J, Li J, Windus TL (2007) Basis set exchange: a community database for computational sciences. J Chem Inf Model 47(3):1045–1052. https://doi.org/10.1021/ci600510j

Swirles B (1935) The relativistic self-consistent field. Proc R Soc Lond Ser A Math Phys Sci 152(877):625–649

Theilacker K, Schlegel HB, Kaupp M, Schwerdtfeger P (2015) Relativistic and solvation effects on the stability of gold (III) Halides in aqueous solution. Inorg Chem 54(20):9869–9875

Visscher L, Dyall KG (1997) Dirac-fock atomic electronic structure calculations using different nuclear charge distributions. At Data Nucl Data Table 67:207

Zuccaccia D, Belpassi L, Macchioni A, Tarantelli F (2013) Ligand effects on bonding and ion pairing in cationic gold(I) catalysts bearing unsaturated hydrocarbons. Eur J Inorg Chem 24:4121–4135. https://doi.org/10.1002/ejic.201300285